Investigation of Grid-Forming and Grid-Following Converter Multi-Machine Interactions Under Different Control Architectures

Luke Benedetti[1], Alexandros Paspatis[2,4], Panagiotis N. Papadopoulos[1,3],
Agustí Egea-Àlvarez[1], Nikos Hatziargyriou[4]
[1]Department of Electronic & Electrical Engineering, University of Strathclyde, Glasgow, Scotland
[2]Department of Engineering, Manchester Metropolitan University, Manchester, United Kingdom
[3] Department of Electrical and Electronic Engineering, University of Manchester, Manchester, United Kingdom
[4]School of Electrical and Computer Engineering, National Technical University of Athens, Athens, Greece

***Abstract*—The proliferation of converter-interfaced generation necessitates the investigation of novel small-signal multi-machine interactions. The flexibility and lack of standardisation of converter control approaches results in a plethora of potential implementations, bringing different dynamics that can interact with each other and existing elements of the power system. This paper performs a small-signal analysis of power systems with the inclusion of grid-forming and grid-following converters for varying combinations of common control architectures, in terms of cascaded control loops, within the literature. Investigations are performed for a two-machine system and the WSCC 9-bus (three-machine) system. As well as interaction identification and characterisation, the impact of varying transmission line lengths, system loading, and generation dispatch are investigated.**

***Index Terms*—Converter, grid-following, grid-forming, interaction, small-signal.**

I. Introduction

The uptake of converter-interfaced generators (CIGs), and subsequent reduction of synchronous generators (SGs), is causing major changes to the dynamic characteristics of the power system [1], [2]. This includes the potential for new dynamic interactions between the wide bandwidth control of the CIG with existing power system elements, each other, and even the electromagnetic dynamics of the network [3], [4]. Consequently, extensive research into potential small-signal multi-machine (or multi-element) interactions is required to capture those with notable influence over the dynamic response or the stability of the power system.

The flexibility of the digital implementation of CIG control results in a huge potential for differing control architectures and parameter tuning. In particular, there are ongoing questions regarding the optimal controller architectures to adopt for grid-forming (GFM) control approaches due to the difficulty with standard tuning practices in high power applications and multi-machine networks [5], [6], while various topologies can be also found in the literature regarding grid-following (GFL) control schemes.

The common approach for realising a GFM scheme relies on a multi-loop control structure, with inner current and voltage controllers (ICC and IVC) regulating filter current and voltage, and an outer power loop responsible for the primary control objectives [7], i.e., voltage and frequency regulation and power sharing. Further adaptations based on the concept of virtual impedance are common but are not considered in this work [3], [8], [9], [10]. Alterations of the multi-loop approach are also met in the literature, with the most common being not including inner loop control schemes, or including only an ICC [11]. In a similar manner, derivatives of the common GFL schemes consisting of a single current controller, may focus on including a further control loop directly regulating the output active and reactive power [12]. However, the impact of adopting each different GFM or GFL control architecture to the stability of the converter-dominated multi-machine power system has not been investigated to the required depth.

The impact of GFM controller architecture choice on the small-signal stability of single machine-infinite bus (SMIB) systems has been investigated in [13]. Additionally, small-signal analyses of the interactions between multiple CIGs have been performed in the literature, including [14] and [15]. However, these do not consider how the choice of controller architecture affects the specific small-signal stability and interactions. In [3], an extensive small-signal analysis is performed to determine the major causes of instability with increasing penetrations of CIGs, considering a generation mixture of SGs, GFMs, and GFLs. They utilise a two-machine system for detailed analysis of interactions between SGs & GFLs, SGs & GFMs, and GFMs & GFLs. They also investigate the WSCC 9-bus and South-East Australian systems but only in terms of stability margins. Our work adds to the analysis in [3] with a comparison of controller architecture combinations. Additionally, comprehensive participation factor (PF) analysis

Financial support is acknowledged from an EPSRC Student Excellence Award Studentship 2437798 (L. Benedetti) and a UKRI Future Leaders Fellowship MR/S034420/1 (P. N. Papadopoulos). All results can be fully reproduced using the methods and data described in this paper and provided references.

of the interactions involving CIG is performed, rather than focusing only on the modes which cause instability.

A small-signal study with two to three CIGs connected to an infinite bus while including or neglecting a GFM, and then including or neglecting an ICC for the GFM, was performed in [16]. They find that reducing the grid-strength causes instability when there is only GFLs (excepting the infinite-bus) or when the GFM includes an ICC. In addition, they highlight that an increasing penetration of GFM compared to GFL ensures stability in their system. Compared to this, the following work considers more controller architecture combinations as well as further parametric variation studies. Additionally, there is no infinite-bus in this work.

The novel contribution of this work is the comparison of potential multi-machine small-signal interactions and the impact of network parametric variations under different combinations of GFM and GFL architectures, supporting discussions regarding the benefits and drawbacks of each controller choice and the potential appearance of instabilities.

Following this introduction, Section II describes and validates the small-signal modelling. Section III details the case studies that are performed, with Section IV displaying the corresponding results. The paper concludes in Section V.

II. Modelling

This section details the models adopted for the network elements, SG, and voltage source converter (VSC). It also describes the controller architecture choices that are utilised for the GFL and GFM control. Finally, the small-signal models are validated against corresponding nonlinear models. Note, the small-signal models are developed in MATLAB 2021b.

A. Network

The passive components of the network are modelled dynamically to account for potential high frequency interactions with converter control [2], [4]. Transmission lines are represented by the π equivalent model and the transformers and loads by series RL impedances.

B. Synchronous Generator

The synchronous generator model adopted is the 8^{th} order linear magnetic model detailed in [17]. The per unit parameters used are those of the Kundur two-area system in Example 12.6 in [18] but with inertia constant of $6.5\ s$ used for all machines. In this work the SG has constant excitation and there is no automatic voltage regulator (AVR), governor-turbine, or power system stabiliser (PSS) connected (excepting Section IV.C).

C. Voltage Source Converter

All connected CIGs include an LCL filter (if the external transformer is considered), as illustrated in Fig. 1. Note, the superscript * corresponds to signals in the converter control reference frame and the arrow represents a dynamic phasor in the dq0 notation [4] as $\vec{x} = x_d + jx_q$. The converter itself is represented by the averaged model, taking the modulation voltage signal, $\vec{v}^*_{cv}$, from the control and applying it to $\vec{v}_{cv}$ via a reference frame transformation. This transform is between the control reference frame, aligned with the internal machine angle, and the system reference frame which is aligned with a chosen reference machine. The resistance, R_f, inductive reactance, $X_{l,f}$, and capacitive reactance, $X_{c,f}$, have values of $0.03\ pu$, $0.08\ pu$, and $13.51\ pu$, respectively.

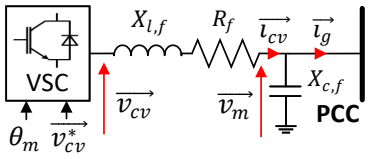

Fig. 1: Voltage source converter with LC(L) filter.

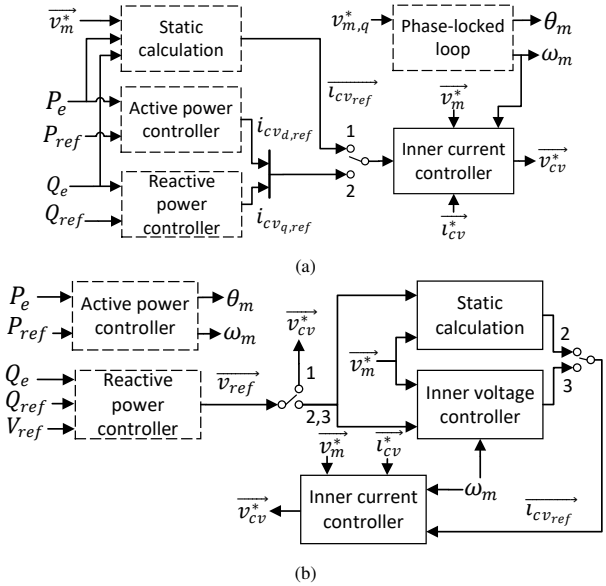

Fig. 2: (a) Grid-following control. Switches: 1=single loop control and 2=double loop control. (b) Grid-forming control. Switches: 1=direct AC voltage control, 2=single inner loop control and 3=double inner loop control. Note, dashed boxes represent controllers considered to be in the outer loop.

D. Grid-Following Converter

For the GFL control realisation, two approaches are often found in the literature, 1) single loop control (SLC) and 2) double loop control (DLC). In the first case, only an inner current controller is required (identical to that of the GFM case presented in [7]), with the current references being calculated through a static calculation based on the power references and the measured voltage [19]. In the second case, an extra control loop is included, generating the current reference values based on PI controllers regulating the output power to their reference value [12]. The described implementation is graphically shown in Fig. 2a. In this work, the proportional and integral gains of the PI controllers are $0.25\ pu$ and $25\ pu$ for both outer controllers, $60\ pu$ and $1400\ pu$ for the PLL, and $1\ pu$ and $10\ pu$ for the ICC. For these controllers, this tuning achieves closed-loop bandwidths of $3.3\ Hz$, $13\ Hz$, and $747.6\ Hz$, respectively. This tuning was based on [20]. The power measurement time constant is $0.0318\ s$.

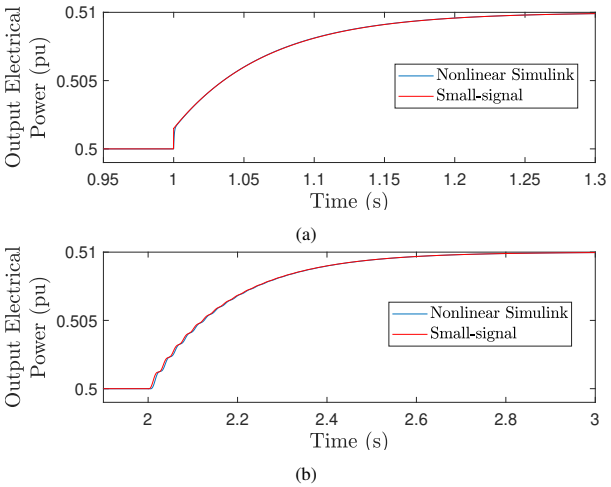

Fig. 3: (a) Grid-following double loop control and (b) grid-forming double inner loop control small-signal model validation.

E. Grid-Forming Converter

Various alternative implementations of GFM control schemes are presented in the literature. Apart from the variety of different droop control schemes, virtual impedances, or the inclusion or not of feed-forward terms [3], [21], [22], the architecture with regards to inner control loops may also vary [11], a fact raising rather important concerns for the stability of CIG-dominated power systems, due to the different timescales of the inner and outer loop control schemes. Hence, three different approaches are considered in this paper for the GFM control realisation, 1) direct AC voltage control (DACVC), 2) single inner loop control (SILC) and 3) double inner loop control (DILC), with their realisation being graphically depicted in Fig. 2b. For the structure of the inner and outer control loops the reader is referred to [7], [11]. Particularly, feed-forward terms are considered, while low-pass filtering of the measured power is used to provide virtual inertia characteristics [23]. Note, the static calculation required for SILC can be regarded as a form of virtual admittance with parameters chosen to compensate for the RL impedance of the VSC output filter [13]. However, this should not be confused with virtual impedance additions used for supplementary control or impedance shaping such as in [8], [9], [10].

Control elements common with the GFL have the same tuning. The droop gain is $0.02\ pu$ and $0.0289\ pu$ for the active and reactive power controllers respectively, based on [3]. The proportional and integral gains for the IVC are $1\ pu$ and $100\ pu$ respectively. This tuning was chosen for sufficient timescale separation from both the ICC and outer controllers, with a resultant closed-loop bandwidth of $471.4\ Hz$ [24].

F. Small-Signal Analysis & Validation of Small-Signal Models

This work utilises eigenvalue analysis including participation factor (PF) calculations, concepts which are well established and understood. The reader is referred to [1], [3], [17], [18] if more information is required.

To validate the accuracy of the developed small-signal model, it is here compared to time-domain results obtained using the MATLAB/Simulink environment. In particular, taking into consideration the more complicated control schemes, i.e., the DLC and DILC, their response both through the small-signal model and the nonlinear time-domain model is compared in Fig. 3 for a SMIB system, effectively validating the developed models towards the following investigations.

III. Case Studies

A two-machine system and the WSCC 9-bus are described in this section along with the case studies applied to them and the approach for generation of system operating points.

A. Two-machine System

The two-machine system is displayed in Fig. 4 with dotted section included. It is based on the Kundur two-area system with G1 and G2 being rated at $1800\ MVA$ and $20\ kV$. The transformers are also rated at $1800\ MVA$ with a voltage base of $20\ kV : 230\ kV$. Also, the loads in area 1 and area 2 are absorbing active and reactive powers of $967\ MW$ and $100\ MVAr$, and $1767\ MW$ and $100\ MVAr$, respectively.

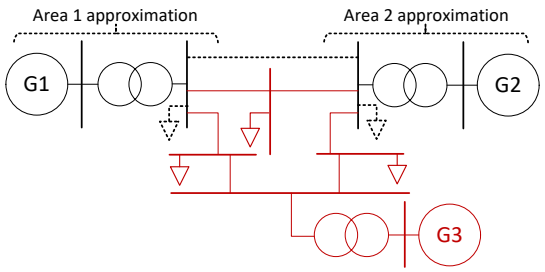

Fig. 4: Study networks: two-machine system when including dotted section or WSCC 9-bus when including red section.

The following generation mixes (G1/G2) are considered:

- SG/GFL (2 combinations of GFL control)
- SG/GFM (3 combinations of GFM control)
- GFM/GFL (6 combinations of GFM/GFL control)
- GFM/GFM (3 combinations of GFM control)

For each of the generation combinations outlined above, the following investigations are performed:

- Interaction analysis (eigenvalues and corresponding PFs) at the base operating point described in Section III-C.
- Varying length of the transmission line interconnection.
- Varying system loading.
- Varying the installed capacity between G1 and G2.

B. WSCC 9-Bus System

Also considered is the WSCC 9-bus system which is displayed in Fig. 4 with the red section included. The generators G1, G2, and G3 are set to be a GFM, GFL, and SG, respectively. The test case parameters can be found in [25].

With this system, the penetration of each type of machine is varied by considering firstly the penetration of SG installed capacity, $SG/Total$, as well as the penetration of GFM installed capacity with respect to the converter installed capacity, $GFM/(GFM + GFL)$.

C. Generation of System Operating Points

The total installed capacity of the system is shared between the machines depending on the specified ratios. This total value is taken as the total installed capacity of the base system, i.e., $1800\ MVA + 1800\ MVA$ for the two-machine system and $247.5\ MVA + 192\ MVA + 128\ MVA$ for the 9-bus system. The change is reflected in the dynamic modelling with a reduction or increase of the machine's rated power. The ratings for the transformers of each generator are updated correspondingly. To vary the loading, a multiplication factor is applied to each load. Finally, the active and reactive power injections of the generators are updated in the power flow case file by extracting the total values for the base case and splitting between the generators, based again on the specified ratios.

The power flow is then run and the results are leveraged to calculate the initial states of the generator dynamic models. This is achieved by setting the derivative terms in the differential equations to zero (i.e., steady state) and solving the resultant system of nonlinear equations.

For both systems, the base case is considered with the installed capacity split evenly between the generators, and a load multiplier of 1. Additionally, the transmission line in the two-machine system is set to $50\ km$.

IV. Results

A. Two-machine System Results

This section details the results obtained from performing the case studies outlined in Section III-A.

For the base operating point (Section III-C), the eigenvalues are displayed in Fig. 5. This includes a plot for each generation mix with the different control architecture combinations distinguished as described by the legend in the Fig. 5 caption.

Also shown, in Fig. 6, are the results of the parametric variations of the transmission line interconnection, system loading, and the ratio of installed capacity (and resultant generation dispatch) between G1 and G2. This includes results for each generation mix with the different control architecture combinations distinguished as described by the legend in the Fig. 6 caption. Note, only the results considered relevant for each case are included, i.e., not all eigenvalues are displayed. The $G1/(G1+G2)$ ratio parametric sweeps are performed for ratios 0.01 up to 0.99 in steps of 0.01, however, from 0.82 onward the power flow does not converge.

Due to space limitations, PFs are not displayed and instead described when relevant. The PF vectors used to characterise modes are representative values taken at the base case which is a limitation of this analysis considering the capability for PFs, similar to the eigenvalues, to vary significantly depending on the system operating point. When describing a mode's PFs, those with value above $2.5\ \%$ are specified.

The modes of interest in this work involve the CIG control. As such, any modes with relative contribution less than $5\ \%$ from CIG control states are neglected. For this purpose only if a mode is found to have less than $5\ \%$ participation from CIG states across all parametric variations will it be neglected. Additionally, modes with damping time constant less than $0.01\ s$ are deemed to have negligible impact on system dynamics and are not considered.

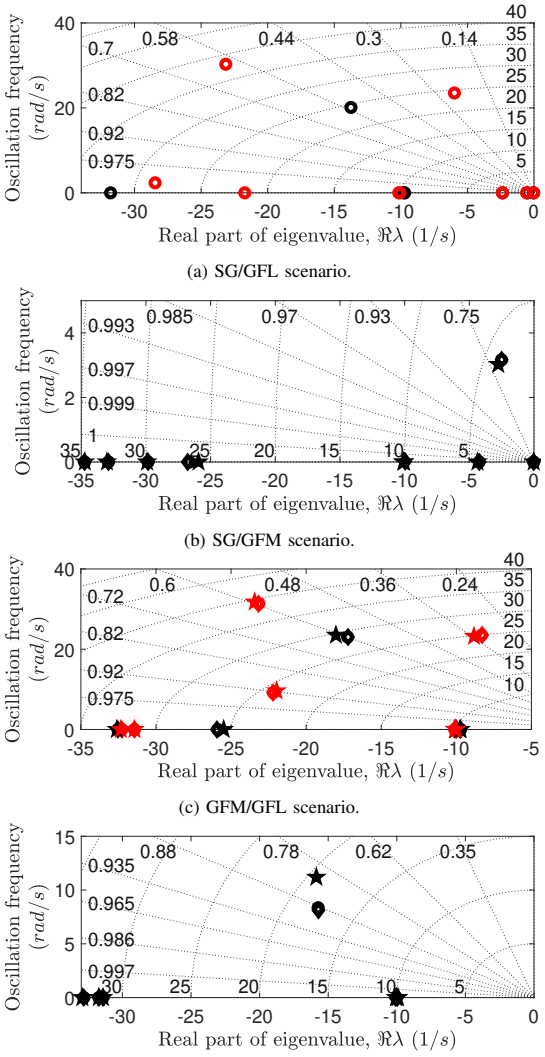

(a) SG/GFL scenario.

(b) SG/GFM scenario.

(c) GFM/GFL scenario.

(d) GFM/GFM scenario (with homogeneous GFM control).

Fig. 5: Eigenvalues with minimum $5\ \%$ contribution from CIG control states and damping time constant above $0.01\ s$ at the base operating point. Legend: black=single loop control (when GFL is present), and red=double loop control; circle=direct AC voltage control (when GFM is present), diamond=single inner loop control, and star=double inner loop control. Note, lines of constant damping ratio and natural frequency are included.

1) SG/GFL: From analysis of the eigenvalue plot in Fig. 5a, the differences between using SLC and DLC for the GFL are clear with the former containing a single oscillatory mode at $-13.8 \pm j20.1$ and the latter containing three at $-6.0 \pm j23.5$, $-23.1 \pm j30.3$, and $-28.5 \pm j2.4$. The SLC oscillation has participation from the GFL's PLL and, to a lesser extent, the SG damper windings. For the DLC, the first two modes that were mentioned have participation from the PLL and outer controllers of the GFL, and the remaining oscillation involves the same controllers and the damper windings of the SG.

From the parametric sweeps in Fig. 6a, it is found that increasing the transmission line length brings a mode towards the unstable region but without reaching it. This is more

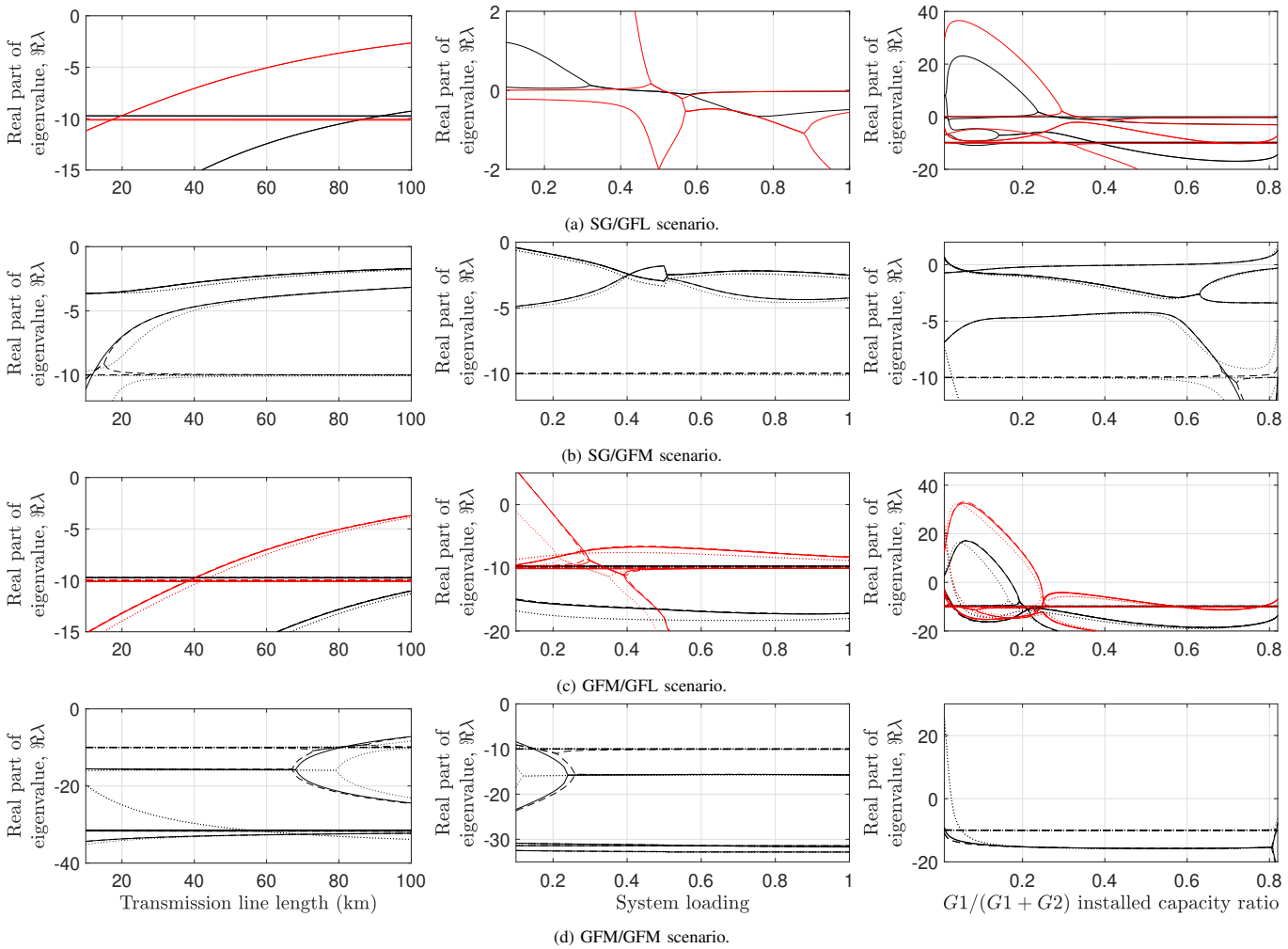

(a) SG/GFL scenario.

(b) SG/GFM scenario.

(c) GFM/GFL scenario.

(d) GFM/GFM scenario.

Fig. 6: Real part of eigenvalues with minimum 5 % contribution from CIG control states for parametric variations. Legend: black=single loop control (when GFL is present), and red=double loop control; solid line=direct AC voltage control (when GFM is present), dashed line=single inner loop control, and dotted line=double inner loop control.

emphasised with the DLC but a similar mode trajectory is seen in the SLC case. These modes are the $-13.8 \pm j20.1$ and $-6.0 \pm j23.5$ modes in the SLC and DLC cases, respectively.

Additionally, at low loading the system is unstable due to a mode with participation from the rotor and damper windings of the SG. Similar non-oscillatory modes are known to exist in Kundur's two area system [18]. It becomes stable at a lower value of loading in the SLC case compared to the DLC case. Note, the PFs of this mode are found to involve the GFL outer controller and PLL at lower loading values, hence the significant impact of the choice of GFL architecture despite the base case PFs suggesting no GFL contribution. This is an example of the difficulty in drawing conclusions for specific interactions due to the variability of PFs.

For the installed capacity variation, both controller architectures cause instability with low SG and high GFL penetration. The mode causing instability in both cases is related to the PLL of the GFL and the rotor and damper windings of the SG. It is seen that when using DLC, the system requires at least 34 % SG penetration to maintain stability while using SLC requires only 28 % SG penetration.

Generally, the SLC case has better stability margins and boundaries for the same modes (i.e., with similar participating states and mode trajectories) than the DLC case. However, using the SLC brings the obvious drawback of an inability to control exactly the active and reactive power.

N.B.: for the parametric sweeps there are instances in which a single mode appears to split (or branch) or where two separate modes seem to combine. This is the result of a single complex-conjugate paired oscillatory mode becoming non-oscillatory resulting in two separate real eigenvalues when splitting and the reverse is true when combining.

2) SG/GFM: From analysis of the eigenvalue plot in Fig. 5b it can be determined that the choice of GFM controller architecture has very limited impact on the dominant modes of the system. There is one oscillatory mode, for all control architectures, at $-2.5 \pm j3.2$, which is found to be an electromechanical interaction between the SG and the GFM. i.e., with participation from the rotor of the SG and the "virtual rotor" of the GFM. Additionally, not shown is an oscillation at $-25.9 \pm j355.3$ present only for the DILC case. This oscillation has participation from the electromagnetic dynamics of the network currents.

The parametric sweeps in Fig. 6b again confirm the lack

of impact of controller architecture choice on the dominant modes in this scenario. Again there is no instability resulting from the transmission line length variation. However, the instability seen at low loading in the SG/GFL scenario is not present in this scenario. At very low SG penetration and high GFM penetration there is instability, but also when there is very high SG penetration and low GFM penetration. The cause of instability for both of these cases is different with the former being the electromechanical interaction between the SG and GFM, and the latter being a non-oscillatory mode involving the SG damper windings and rotor.

3) GFM/GFL: The eigenvalue plot in Fig. 5c can be compared to the plot for the SG/GFL scenario with one oscillation for the SLC at approximately $-17.2 \pm j23.0$ and the DLC containing three oscillations at $-8.3 \pm j23.5$, $-22.2 \pm j9.2$ and $-23.2 \pm j31.4$. However, the least damped oscillation is this time seen to have a greater stability margin with respect to the eigenvalue real part. The dominant states of these modes resemble their SG/GFL counterparts but where in the SG/GFL case these modes had contribution from the SG rotor and damper windings, in this case it is instead contribution from the GFM rotor. Additionally, several non-oscillatory modes with low damping time constant, that correspond primarily to the SG damper windings, are no longer present.

The impact of GFL controller architecture choice is clearly greater on these dominant modes compared to the choice for the GFM. However, there is a slight improvement in terms of damping for the least damped mode when using DILC as opposed to DACVC or SILC.

The parametric sweeps in Fig. 6c again highlight the similarities to the SG/GFL case and the limited impact of GFM controller architecture choice. However, the loading variation reveals no instability for the SLC at low loading values and a greatly increased stability region for the DLC. This is due to the lack of the SG damper windings/rotor mode that caused the issues in the SG/GFL case. Additionally, the relative lack of impact of the choice of GFM architecture is again observed. There is the slight impact of using DILC, especially at low loading (where this prevents instability) and low GFM penetration scenarios.

4) GFM/GFM: The eigenvalue plot in Fig. 5d can be compared to the corresponding plot for the SG/GFM scenario. There is again a single oscillatory mode which in this case is much more damped and at a higher frequency, at approximately $-15.8 \pm j11.2$. In this scenario, this electromechanical mode is an interaction between the virtual rotors of the GFMs. Also in this scenario there is another high frequency oscillation (not shown), at $-31.0 \pm j328.7$, with participation from the current dynamics of the network. Again, the lack of a SG means the removal of several non-oscillatory modes with low damping time constant.

From Fig. 6d, this scenario poses no threat to stability under the range of parametric variations, other than at very low penetrations of G1. In this exceptional circumstance, only the use of DILC causes the instability and it is the oscillatory mode described earlier that is the culprit.

5) Two-Machine System Results Discussion: A high level conclusion is that, for the specific system set up, the small-signal stability is affected much more by the choice of GFL architecture than the choice of GFM architecture (although there is small impact when adopting DILC). This is likely due to the fact that the interactions that cause stability issues in this system are generally related to slower dynamic phenomena, of which the different GFL control architecture choices are focused. Contrastingly, the differing controller architecture choices for the GFM involve the inclusion of the inner controllers which ideally are sufficiently decoupled from the slower dynamics of the primary control.

Additionally, although not observed from Fig. 6, the frequency of the modes can vary in response to the parametric variations. As an example, in the GFM/GFL case, when the GFL uses SLC and the GFM uses DILC, there is a mode which is unstable at low penetrations of $G1/(G1+G2)$. This mode varies in frequency from $6.74\ Hz$ to $2.30\ Hz$, and when using DACVC or SILC, a similar mode is seen which varies from $10.41\ Hz$ to $1.82\ Hz$ (although this mode is never unstable). However, such a variation is not guaranteed. For example, in the transmission line length sweep in Fig. 6a the highlighted modes, which are at $-13.8 \pm j20.1$ and $-6.0 \pm j23.5$ in the base case, are found to have relatively constant oscillation frequency as the parameter varies. This highlights the care required when performing interaction analyses as well as the wide range of frequencies that may require monitoring in converter-dominated systems.

B. WSCC 9-bus System Results

The resulting stability margins from varying the installed capacity of each generator, as described in Section III-B, are displayed in Fig. 7. The immediately obvious conclusion is that, in this system, the stability is affected much more by the choice of GFM controller architecture than that of the GFL.

The choice of GFL architecture has a small impact on stability boundaries, with the use of DLC causing an additional region of instability when the SG and GFM penetrations are low (i.e., the GFL penetration is high). The modes found to be causing instability in this region are non-oscillatory and attributed to the PLL and outer controllers of the GFL. When the GFM utilises DACVC or SILC, the use of DLC reduces the instability region at high SG and GFM penetration (region which doesn't exist when using DILC for the GFM). The cause of instability in this region is a non-oscillatory mode with participation from the SG rotor and damper windings.

The significant unstable region existing when using SILC, generally towards low penetration of SG and high penetration of GFM, is attributed to a very high frequency mode (above 2 kHz) with participation from the output LC filter of the GFM.

The unstable region when using DILC is opposing that when using the SILC, with high SG penetration and low GFM penetration causing instability. For this case, the instability is caused by an oscillation ranging from $9.46\ Hz$ to $12.53\ Hz$ with participation from the GFM active power controller, voltage magnitude controller, and inner voltage controller.

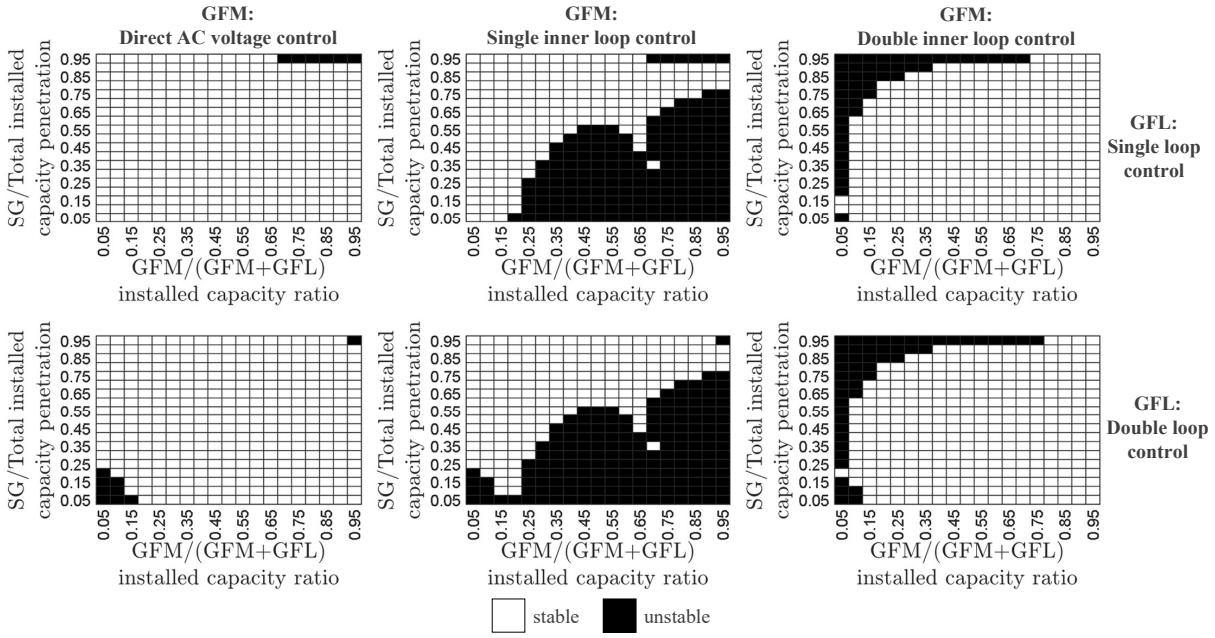

Fig. 7: Stability maps for 9-bus system considering variation of generator penetrations. Y-axis gives proportion of total installed capacity coming from the synchronous generator. X-axis gives proportion of converter installed capacity coming from the grid-forming converter. Therefore, the remainder of the installed capacity comes from the grid-following converter.

It can be noted that, for this system setup, none of the instability inducing modes are multi-machine interactions.

C. Impact of Including Synchronous Generator Controllers

As has been revealed already, the results of these types of small-signal interaction analyses are very sensitive to the system under test. However, SGs are generally always equipped with some form of AVR and associated exciter. Additionally, they will often utilise a PSS. Therefore, these controllers have been added to the SG to determine how this might impact the previously discussed results. The DC1A AVR and exciter combination is adopted as well as the PSS1A PSS. The per unit parameters used for these controllers are taken from Examples 12.6.b.i and 12.6.b.iv of [18], respectively.

The eigenvalues displayed in Figs. 5a and 5b were largely unaltered other than the addition of an oscillatory mode of approximately $-0.3 \pm j1.4$ and $-0.61 \pm j0.5$, respectively. The GFL controller architecture choice has a small influence on this mode. It was seen to have participation primarily from the SG damper windings, rotor, AVR, and PSS. For the SG/GFL base case the participation from CIG states is only 1.11 % and 0.52 % when using SLC and DLC, respectively. For the SG/GFM case there is 2.36 % contribution from CIG states.

As an example of the influence of these controllers on the results of the parametric variations, Fig. 8 displays the loading sweep for the SG/GFM case. It is observed that the trajectories seen in Fig. 6b are impacted little but there are two additional modes with low stability margin. In particular, one mode is unstable for low loading values. This is a non-oscillatory mode related to the SG damper windings, AVR, and GFM rotor when unstable, and related mostly to the PSS at high values of loading. Checking all system modes (i.e., not just those

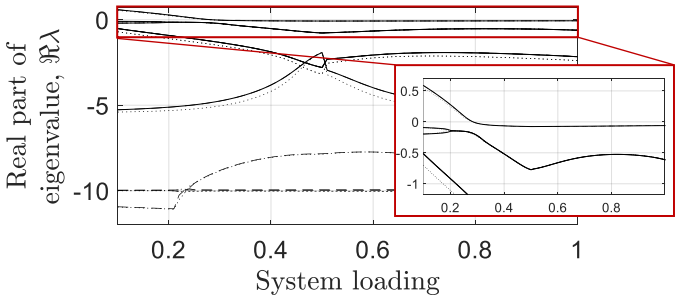

Fig. 8: Real part of eigenvalues with minimum 5 % contribution from CIG control states for variation of loading in SG/GFL case with inclusion of AVR, exciter and PSS.

with contribution from CIG) reveals that this instability does not occur in the system without SG controls. The other mode with low stability margin is the aforementioned oscillation.

These results highlight the importance of including all relevant controllers in small-signal interaction analyses.

V. Conclusions

This paper investigates the small-signal interactions that might occur in two multi-machine systems, namely a two-machine system and the WSCC 9-bus system. It also explores the impact on mode stability and trajectories as a result of varying system parameters. There is a focus on the impact of controller architecture variations with respect to the inclusion or neglection of cascaded controllers.

For the two-machine system, the choice of GFL controller architecture is of significant importance, with regards to the number of oscillations and influence over stability margins. In particular, the use of DLC tends to reduce the region of stability when considering low loading and low SG (or GFM) penetration. The inclusion of a GFM tends to increase stability

regions compared to scenarios with either GFL or SG in its place. Additionally, the choice of controller architecture for the GFM has limited influence in this system.

For the 9-bus system, the GFL control architecture choice has less of an impact but does result in a small region of instability at low SG and GFM penetrations when using DLC. Contrastingly, the GFM controller architecture choice in this case has a significant impact, with SILC resulting in a large region of instability with low SG and high GFM penetrations, related to a high frequency mode with contribution from the CIG output filter. When using DILC there is a region of instability towards high SG and low GFM penetration caused by a ($9.46\ Hz$ to $12.53\ Hz$) mode involving the primary control and inner voltage control of the GFM.

The variability of modes (and their participation factors) with regards to system parameters and operating points, controller tunings and architecture choice, amongst others, makes generalising conclusions for these types of analyses very challenging. This is strengthened through a study in which the AVR and PSS were added to the SG, revealing the addition of an instability at low loading for the SG/GFM case which is not present without these controllers. Therefore, it is recognised that there is a crucial need for performing extensive multi-machine interaction investigations for more complex systems with different layouts, controllers, tuning, operating points, and more. This is true not just for small-signal interaction studies but also the expansion to nonlinear analysis such as investigation of fault ride-through capabilities.

Despite these difficulties, this paper illuminates potential small-signal interactions and mode trajectories from parametric variations, furthering discussions regarding the benefits and drawbacks of GFL and GFM controller architecture choices. As a general note, the fact that very different behaviours are observed raises an important point about potential effects coming from specific control structure choices and the need to describe the implementation of GFM and GFL control in more detail for system stability studies. In addition, converter connected units through various vendors with different implementations might exist in different networks, making a unique recommendation challenging.

REFERENCES

[1] N. Hatziargyriou, J. V. Milanović, C. Rahmann, V. Ajjarapu, C. Cañizares, I. Erlich, D. Hill, I. Hiskens, I. Kamwa, B. Pal, P. Pourbeik, J. J. Sanchez-Gasca, A. Stanković, T. V. Cutsem, V. Vittal, and C. Vournas, "Definition and classification of power system stability – revisited & extended," *IEEE Trans. on Power Systems*, vol. 6, pp. 3271 – 3281, 2021.

[2] Y. Gu and T. C. Green, "Power system stability with a high penetration of inverter-based resources," *Proceedings of the IEEE*, vol. 111, no. 7, pp. 832–853, 2023.

[3] U. Markovic, O. Stanojev, P. Aristidou, E. Vrettos, D. Callaway, and G. Hug, "Understanding small-signal stability of low-inertia systems," *IEEE Transactions on Power System*, vol. 36, pp. 3997–4017, 2021.

[4] R. Henriquez-Auba, J. D. Lara, C. Roberts, and D. S. Callaway, "Grid forming inverter small signal stability: Examining role of line and voltage dynamics," in *IECON Proceedings (Industrial Electronics Conference)*, Singapore, 2020, pp. 4063–4068.

[5] T. Qoria and X. Guillaud, "Grid-forming control suitable for large power transmission system applications," Dec. 2021. [Online]. Available: http://dx.doi.org/10.36227/techrxiv.17089199.v1

[6] A. Narula, M. Bongiorno, and M. Beza, "Comparison of grid-forming converter control strategies," in *2021 IEEE Energy Conversion Congress and Exposition (ECCE)*, Vancouver, BC, Canada, 2021, pp. 361–368.

[7] N. Pogaku, M. Prodanovic, and T. C. Green, "Modeling, analysis and testing of autonomous operation of an inverter-based microgrid," *IEEE Transactions on Power Electronics*, vol. 22, no. 2, pp. 613–625, 2007.

[8] X. Wang, Y. W. Li, F. Blaabjerg, and P. C. Loh, "Virtual-impedance-based control for voltage-source and current-source converters," *IEEE Transactions on Power Electronics*, vol. 30, no. 12, pp. 7019–7037, 2015.

[9] L. Huang, H. Xin, H. Yuan, G. Wang, and P. Ju, "Damping effect of virtual synchronous machines provided by a dynamical virtual impedance," *IEEE Transactions on Energy Conversion*, vol. 36, no. 1, pp. 570–573, 2021.

[10] D. Yang, X. Ruan, and H. Wu, "Impedance shaping of the grid-connected inverter with LCL filter to improve its adaptability to the weak grid condition," *IEEE Transactions on Power Electronics*, vol. 29, no. 11, pp. 5795–5805, 2014.

[11] K. Vatta Kkuni, S. Mohan, G. Yang, and W. Xu, "Comparative assessment of typical control realizations of grid forming converters based on their voltage source behaviour," *Energy Reports*, vol. 9, pp. 6042–6062, 2023.

[12] L. Huang, C. Wu, D. Zhou, and F. Blaabjerg, "Comparison of three small-signal stability analysis methods for grid-following inverter," in *2021 International Aegean Conference on Electrical Machines and Power Electronics & 2021 International Conference on Optimization of Electrical and Electronic Equipment*, 2021, pp. 34–41.

[13] M. Beza and M. Bongiorno, "Impact of converter control strategy on low- and high-frequency resonance interactions in power-electronic dominated systems," *International Journal of Electrical Power & Energy Systems*, vol. 120, p. 105978, 2020.

[14] R. Rosso, S. Engelken, and M. Liserre, "Robust stability investigation of the interactions among grid-forming and grid-following converters," *IEEE Journal of Emerging and Selected Topics in Power Electronics*, vol. 8, pp. 991–1003, 2020.

[15] A. Sajadi, R. W. Kenyon, M. Bossart, and B. M. Hodge, "Dynamic interaction of grid-forming and grid-following inverters with synchronous generators in hybrid power plants," in *2021 IEEE Kansas Power and Energy Conference, KPEC 2021*, Manhattan, KS, USA, 2021.

[16] Y. Lamrani, F. Colas, T. Van Cutsem, C. Cardozo, T. Prevost, and X. Guillaud, "On the respective contributions of different grid-forming controls to small-signal stability," Feb. 2023. [Online]. Available: http://dx.doi.org/10.36227/techrxiv.22006310.v1

[17] P. W. Sauer and M. A. Pai, *Power System Dynamics and Stability*. The University of Illinois, 1997.

[18] P. Kundur, *Power System Stability and Control*, 3rd ed. McGraw-Hill, 2017.

[19] A. G. Paspatis and G. C. Konstantopoulos, "Voltage support under grid faults with inherent current limitation for three-phase droop-controlled inverters," *Energies*, vol. 12, no. 6, 2019.

[20] L. Fan, Z. Miao, D. Ramasubramanian, and H. Ding, "Operational challenges of solar pv plus storage power plants and modeling recommendations," *IEEE Open Access Journal of Power and Energy*, vol. 10, pp. 477–489, 2023.

[21] G. Denis, T. Prevost, P. Panciatici, X. Kestelyn, F. Colas, and X. Guillaud, "Improving robustness against grid stiffness, with internal control of an AC voltage-controlled VSC," in *2016 IEEE Power and Energy Society General Meeting (PESGM)*, Boston, MA, USA, 2016, pp. 1–5.

[22] W. Du, Z. Chen, K. P. Schneider, R. H. Lasseter, S. P. Nandanoori, F. K. Tuffner, and S. Kundu, "A comparative study of two widely used grid-forming droop controls on microgrid small-signal stability," *IEEE Journal of Emerging and Selected Topics in Power Electronics*, vol. 8, no. 2, pp. 963–975, 2020.

[23] S. D'Arco and J. A. Suul, "Equivalence of virtual synchronous machines and frequency-droops for converter-based microgrids," *IEEE Transactions on Smart Grid*, vol. 5, no. 1, pp. 394–395, 2014.

[24] S. D'Arco, J. A. Suul, and O. B. Fosso, "Automatic tuning of cascaded controllers for power converters using eigenvalue parametric sensitivities," *IEEE Transactions on Industry Applications*, vol. 51, no. 2, pp. 1743–1753, 2015.

[25] P. M. Anderson and A. A. Fouad, *Power System Control and Stability*, 2nd ed. Wiley-IEEE Press, 2003.